ELSEVIER

Journal of Power Sources 89 (2000) 237–243

JOURNAL OF POWER SOURCES

www.elsevier.com/locate/jpowsour

^{7}Li NMR study of intercalated lithium in curved carbon lattices ☆

R.E. Gerald II, R.J. Klingler [a,*], G. Sandí [a], C.S. Johnson, L.G. Scanlon [b], J.W. Rathke

[a] *Chemical Technology and Chemistry Divisions, Argonne National Laboratory, 9700 S. Cass Avenue, Argonne, IL 60439-4837, USA*
[b] *Air Force Research Laboratory, Battery Branch, Wright-Patterson Air Force Base, OH 45433-7251, USA*

Received 4 October 1999; accepted 10 December 1999

Abstract

A device was invented that permits nuclear magnetic resonance (NMR) analysis of the internal elements of a coin cell battery. The *Coin Cell Battery Imager* was used to record wideline ^{7}Li NMR spectra of the lithium ions that were electrochemically intercalated into three different types of carbon-based materials. The samples included graphite, corannulene, and carbon derived from sepiolite clay. All samples were excised from 2032-size coin cells that were cycled multiple times and left in a discharged state (i.e., fully lithiated). A comparison of the ^{7}Li NMR spectra recorded for the three carbons revealed that the curved carbon lattice derived from sepiolite affected the lithium resonances in a manner similar to that observed for the curved molecule corannulene, while both differed from the flat lattice of graphite. In addition, it was possible to observe lithium dendrites on the surface of a hard carbon electrode even in the presence of a large lithium counter electrode using NMR imaging techniques.

Keywords: ^{7}Li NMR study; Intercalated lithium; Curved carbon lattices; Coin cell battery

1. Introduction

Carbonaceous materials have received considerable interest for use as anodes ever since Sony introduced the lithium-ion battery [1,2]. Carbon containing systems are noted for potential safety and reliability advantages because the carbon anodes are less prone to form dendrites than metallic lithium anodes. Most investigations have utilized carbon materials that are available from existing sources such as natural graphite, cokes, carbon fibers, non-graphitizable carbon, and pyrolitic carbon [3–7]. In these studies, high lithium capacities have been found to be associated with either disorder [8–10] or the presence of hydrogens [11–13].

An alternative avenue is the custom synthesis of carbons specifically tailored for use as anodes in lithium-ion batteries. This latter approach provides predictable control over critical properties such as the surface area or the porosity. Previously, Sandí et al. [14–16] employed pillared clays with known interplanar spacing as templates for the synthesis of custom carbon anode materials. More recently, they have focused on the concept that carbons with curved lattices can exhibit enhanced lithium capacity over that of graphite. This idea was underscored by computational studies of endohedral lithium complexes of buckminster fullerene, C_{60} [17,18]. It was found that the interior of the C_{60} molecule was large enough to easily accommodate two or three lithiums. Furthermore, the curved ring structure of the C_{60} molecule facilitated the close approach, 2.96 Å, of the lithiums even in the trilithiated species. This is significantly closer than the interlithium distance in the stage-one graphite complex LiC_6 and suggests that lithium anode capacities may be improved over graphitic carbon by synthesizing carbons with curved lattices that approximate a portion of a buckey ball [19].

☆ The submitted manuscript has been created by the University of Chicago as Operator of Argonne National Laboratory (''Argonne'') under Contract No. W-31-109-ENG-38 with the US Department of Energy. The US Government retains for itself, and others acting on its behalf, a paid-up, non-exclusive, irrevocable worldwide license in said article to reproduce, prepare derivative works, distribute copies to the public, and perform publicly and display publicly, by or on behalf of the Government.

* Corresponding author. Tel.: +1-630-252-9960; fax: +1-630-252-9373.

E-mail address: klingler@cmt.anl.gov (R.J. Klingler).

0378-7753/00/$ - see front matter
PII: S0378-7753(00)00435-3

This concept was experimentally tested using corannulene ($C_{20}H_{10}$) as a model electrode material. Corannulene is a discrete molecular species. Its X-ray crystal structure confirmed the anticipated bowl-shaped geometry in which none of the five six-member carbon rings are coplanar with the others [20]. The structure of corannulene is best described as the top section of a buckey ball. Anodes were fabricated from corannulene and tested vs. lithium metal in a standard coin cell. The reversible lithium capacity, 602 mA h/g, was notably higher than that for fully lithiated graphite LiC_6, 372 mA h/g [21]. In addition, computational investigations of lithiated corannulene indicated two remarkable features. First, the computations predicted orbital multiplicities of 2 or 4. This was in agreement with the ^{7}Li nuclear magnetic resonance (NMR) spectra of the lithiated corannulene anode, which were found to be consistent with a paramagnetic complex [21]. Second, the charge transfer from the lithiums to the corannulene ring system was calculated to be quite small. Consistently, workers at Sony have also calculated that reversible lithium intercalation in hard carbon is associated with geometries that induce a small degree of electron transfer to the carbon layers [22]. These computational results suggest that low positive charge density on the lithium centers results in high reversible lithium intercalation capacities by facilitating lithium cluster formation.

The first synthetic carbon to be designed based on these concepts was produced using sepiolite as an inorganic template [23]. Sepiolite is a fibrous phyllosilicate clay with elongated channels, 3.7×10.6 Å, that run parallel to the length of the fibers. These channels serve as a template for the pyrolytic formation of carbon. Well-formed carbon fibers of 1–2 μm in length are produced after the inorganic matrix is removed by acid treatment. These carbon fibers are composed of a microporous network structure with a mean pore radius of 6.8 ± 0.5 Å, which was measured by small angle scattering techniques [23]. This curvature is of the same molecular dimension as the corannulene molecule, and the latter is used as a model for the sepiolite-derived synthetic carbon. Consistently, the reversible lithium capacity of 633 mA h/g for the carbon obtained using sepiolite as the template is similar to that found for corannulene itself. Importantly, both values are significantly higher than graphite.

In this study, we compare the ^{7}Li NMR spectral features of the lithium intercalation product from the carbon fibers synthesized using a sepiolite template with the corresponding lithium intercalates of corannulene and a graphite standard. We also introduce a new electrochemical-NMR cell with the dimensions of a standard 2032-size coin cell. A salient feature of this NMR cell is that the electrode material is mounted directly on the central conductor of the NMR detector circuit for optimum signal sensitivity. This arrangement allows wideline ^{7}Li NMR spectra to be obtained on carbon samples as small as 10 mg. In addition, the new coin cell geometry employs an outer torodial cavity of the type that we have used for in situ NMR imaging of battery systems [24–30].

2. Experimental

2.1. Carbon synthesis

The carbon sample was prepared using sepiolite as a template according to the reported procedure [23]. The sepiolite clay was obtained from Yunclillos (Toledo, Spain), provided by TOLSA: Ethylene and propylene (AGA, 99.95%) were loaded in the gas phase and pyrolyzed in one step. A three-zone furnace was used. Quartz boats containing sepiolite were placed within a quartz tube. The tube was initially flushed with nitrogen for about 3 h. The gas was then switched to propylene or ethylene and the gas flow was maintained at about 5 cm^3/min. The temperature of the oven was gradually increased from room temperature to 700°C at approximately 5°C/min. The oven was then held at that target temperature for 4 h. The clay from the loaded/pyrolyzed sepiolite sample was removed using HF, previously cooled at 0°C to passivate the exothermic reaction. The resulting slurry was stirred for about 1 h. It was then rinsed to neutral pH and refluxed with concentrated HCl for 2 h. The sample was washed with distilled water until the pH was > 5 to ensure that there was no acid left. The resultant carbon was oven dried overnight at 120°C.

2.2. Electrode fabrication

The electrodes were produced by standard methods [31]. The carbon electrodes were made by mixing 84% by weight of the sample with 6% carbon black and 10% of a polytetrafluoroethylene suspended in water (60% m/m solution, PTFE 30, DuPont). The resulting mixture was dried at 120°C overnight, pressed against copper mesh (9/16″ diameter), dried in vacuo at 85°C, and weighed. Two carbon electrodes were built and cycled in a conventional 2032-size coin cell. The 2032-size coin cells (Hohsen) were constructed in a He-filled glovebox (Vacuum Atmospheres, < 2 ppm O_2) with a disk of Li metal foil (FMC) as the negative electrode, and the sepiolite-derived carbon sample as the positive electrode in this configuration. The electrolyte was 1 M $LiPF_6$ in ethylene carbonate:diethylcarbonate (1:1, Merck). A Celgard 2300 microporous membrane was used as the separator. Electrochemical galvanostatic cycling tests were conducted using a Maccor Series 4000 Battery Tester. The cells were cycled 5 times at a current density of 0.125 mA/cm^2 between 1.5 and 0 V vs. the Li metal foil electrode. After cycling, each coin cell was left in a different state-of-charge condition to reflect either a Li-intercalated condition or its opposite. The electrodes were labeled as electrode 1 and electrode 2. Electrode 1 is the lithiated type (OCV =

0.083 V vs. Li) and had a final active weight of 12.5 mg. Electrode 2 (delithiated type) had an OCV = 1.211 V vs. Li and a final weight of 13.5 mg.

The carbon disks were removed from the cell that were used for recording the cycling data and placed intact into the NMR cell. The NMR coin cell compartment has the dimensions of a standard 2032-size coin cell to facilitate sample transfer of this type. For these ex situ experiments, the lithium counter electrode and the Celgard separator were not transferred to the NMR coin cell. The signal from the Li^+ ions in the residual electrolyte appears as a sharp resonance at 0 ppm. This resonance was used as an internal reference for the ^7Li chemical shift. In the future, it should be possible to spatially resolve the intercalated lithium in the electrode from the lithium in the electrolyte on the basis of distance resolution using rotating frame NMR imaging techniques. This will require calibration of the B_1 field dependence of the new flat coin cell geometry.

2.3. Electrochemical-NMR cell

The electrochemical cell was designed to provide in situ NMR observations of an active electrochemical cell to facilitate studies such as electrode staging effects. The dimensions of the cell were chosen to mimic the configuration of a standard 2032-size coin cell. The active cell components are contained within a Teflon® housing. These components are depicted in Fig. 1, and will be described beginning at the back of the cell. The most important element is the solid copper disk that serves as the current collector for the electrode material, which in this case would consist of a carbon disk prepared as described above. Notably, this solid copper disk also serves as the central conductor in the NMR detector circuit. Copper leads are threaded into the top and bottom edges of the copper disk to provide electrical contact. Importantly, the close proximity of the carbon sample to the NMR detector results in optimum NMR signal sensitivity. Next, the NMR coin cell accommodates a membrane separator and a counter electrode. The counter electrode in these experiments consists of a lithium disk that is punched from a sheet of lithium foil. Finally, at the other end of the stacked internal components, there is a copper mesh current collector that directly contacts the counter electrode. External electrical contact to the mesh current collector is provided by a wire that protrudes through the front of the Teflon® end cap. This end cap is held in place by six nylon machine screws. All of the cell components were constructed of non-magnetic materials to minimize any distortions in the B_0 field homogeneity for the NMR experiments. Standard graphite electrodes have been cycled using the Teflon® coin cell outside the magnet in control experiments with acceptable performance and reversibility through more than 10 cycles. As noted above, the membrane separator and the lithium counter electrode that are depicted in Fig. 1 were not actually employed in the NMR spectroscopic measurements to minimize the signal due to Li^+ ions in the electrolyte. In this case, the extra void space due to the absence of the membrane and the counter electrode was filled with polyethylene spacers.

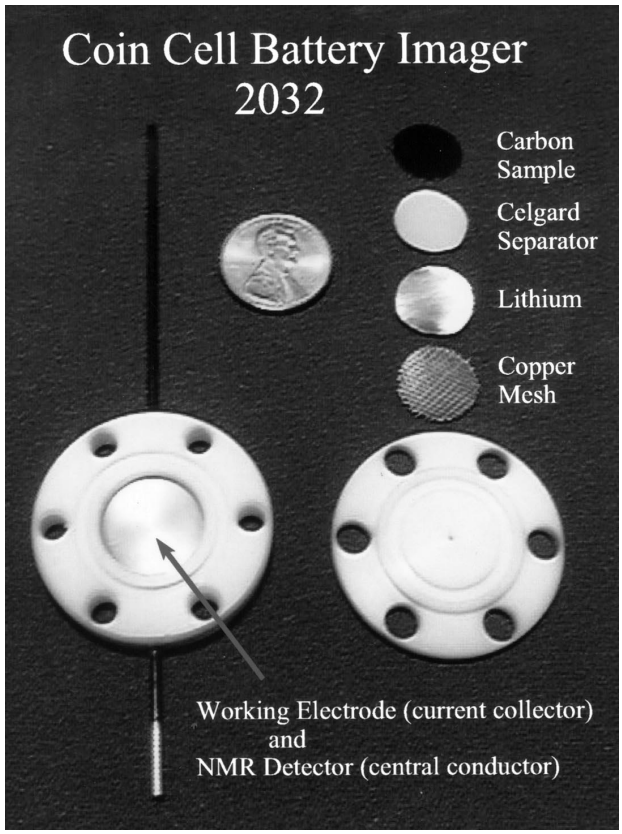

Fig. 1. Photograph of the coin cell battery imager.

The Teflon® encased NMR coin cell is mounted within an outer toroid cavity as shown schematically in Fig. 2. This cavity provides the return path for the current that flows in the NMR detector circuit. In addition, the outer toroid cavity isolates the internal contents from the atmosphere. Standard gas connections allow for experiments at elevated pressures. Indeed, related toroid cavities are routinely employed in our group for in situ NMR investigation of catalytic reaction mechanisms at temperatures ranging to 250°C and pressures up to 300 atm [26]. Also shown in Fig. 2 is an alternative electrochemical-NMR cell design with cylindrical symmetry. The cylindrical geometry provides a well-defined radio frequency B_1 field gradient, which can be exploited for NMR imaging methods. We have used cylindrically symmetric cells of this type for the in situ NMR imaging of the electrolyte depletion layers that form in polymer electrolytes adjacent to the working electrode [26,28]. A cylindrically symmetric cell of the type depicted in Fig. 2 was used in this study to image lithium dendrite formation on the surface of a hard carbon electrode. The toroid cavity fits within a specially fabricated oven. The construction of the oven minimizes the stray magnetic field that is generated by the oven current.

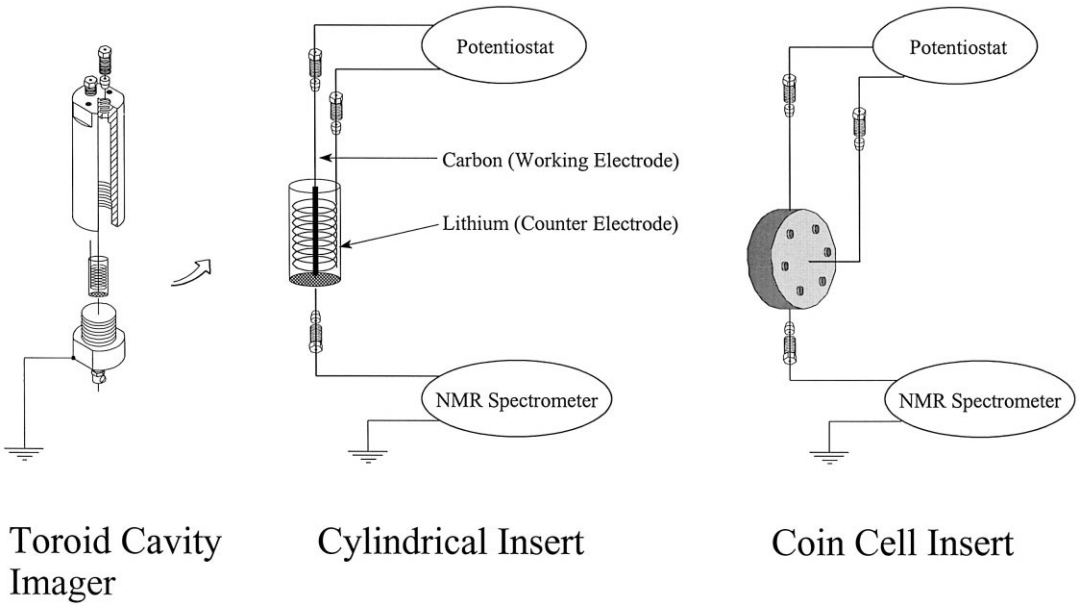

Fig. 2. Schematic layout of the toroid cavity apparatus for the in situ NMR imaging of electrochemical cells.

The entire assembly fits within a wide-bore 89 mm superconducting magnet.

2.4. NMR parameters

^{7}Li NMR spectra were recorded at room temperature by using a ^{UNITY}INOVA-300 WB spectrometer at the following settings: spectrometer frequency, 116.581280 MHz; spectral width, 500 kHz; radio frequency pulse duration, 12 μs; 4096 data points recorded in quadrature, zero-filled to 16,384 data points prior to Fourier transformation; recycle delay, 10.0 s; 1024 (graphite), 4096 (sepiolite) transients per spectrum. One-dimensional NMR spectra were processed with 100 Hz line broadening. No first-order phase correction was applied. The spin-lattice relaxation time constant for ^{7}Li nuclei in the sepiolite sample was not determined, however, a series of experiments with different recycle delays showed that signal saturation was not prevalent for recycle delays as short as 0.250 s.

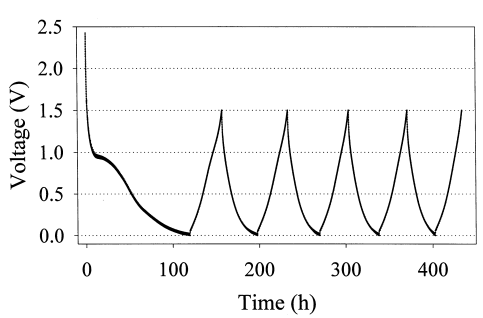

Fig. 3. Voltage profile of an electrode made from carbon fibers that were synthesized in the channels of a sepiolite clay. Voltage range is from 0 to 1.5 V vs. Li^{0} for cycles 2–5.

3. Results and discussion

3.1. Cycling data

The voltage profiles of electrode 2 are provided in Fig. 3. The capacity data are summarized in Table 1. It is clear that there is a high irreversible capacity obtained in the first cycle. This irreversibility can be associated with the formation of a passive layer on the surface of the carbon, which is expected to be enhanced by the presence of several organic active groups. The nature of these groups is under investigation. After the second cycle, the efficiency of the cell increased to more than 90%, and reached almost 97% at the end of the fifth cycle. This is a much higher value than that reported for graphite based anodes, where a utilization of 70–80% was found [21,32]. A higher reversible lithium capacity, 633 mA h/g, was obtained for the sepiolite-derived carbon at a slower charging rate, C/20, and an expanded voltage range, 2.5 to 0 V [23].

Table 1
Specific capacity for the carbon electrode with a voltage profile shown in Fig. 3

Cycle number	Charge capacity (mA h/g)	Discharge capacity (mA h/g)
1	553	1759
2	524	594
3	496	536
4	483	507
5	460	466

3.2. ^{7}Li NMR spectroscopy

The X-ray diffraction pattern previously reported for the sepiolite-derived carbon is indicative of a highly disordered carbon. In addition, the transmission electron micrographs (TEM) clearly revealed well-defined carbon tubes with little or no graphitic character [23]. An alternate characterization of the latter issue is afforded by ^{7}Li NMR spectroscopy because the spectral signature for stage-one graphite intercalate LiC_6 is established [33–35], and it is frequently observed in studies on other carbon materials [36–38]. The spectrum for lithiated graphite obtained in our NMR coin cell is shown in trace A of Fig. 4. The sharp resonance at 0 ppm, which has been marked by a dashed line is due to Li^+ ions from the residual electrolyte. More importantly, the spectrum in trace A exhibits a central transition with a Knight shift of 46.7 ppm and an associated pair of satellites with a quadrupole coupling constant of 47.3 kHz. These values compare quite favorably with literature values for intercalated graphite [33–35]. Significantly, this 47 ppm signature is noticeably absent from the spectrum for the lithiated carbon tubes obtained from sepiolite in trace B of Fig. 4. The ^{7}Li NMR results are in agreement with the TEM data in that there is no detectable graphitic character to the sepiolite-derived carbon.

Two additional spectral signatures are prevalent in the ^{7}Li NMR literature for lithiated carbons. First, for some hard carbons that were heat treated at temperatures near 1000°C, it was reported that resonances were found in the 80–110 ppm range [39–41]. These relatively high shift values are interesting because they are much closer to the Knight shift of metallic lithium, 260 ppm, than the resonance value for lithiated graphite, 47 ppm [33]. This spectral signature is not present in the lithiated carbon tubes that were derived from sepiolite. Second, a very common feature that was observed in a wide range of carbon materials is a ^{7}Li resonance that falls in the 5–20 ppm range [42–46]. The exact NMR shift seems to vary with the prior heat treatment of the carbon [45] and the staging of the electrode material [46]. Quadrupole satellites are usually not resolvable for this lithium signature. The carbon tubes that were synthesized from sepiolite and subsequently lithiated do have a resonance in this chemical shift range at 13.5 ppm. Again, the sharp resonance at 0 ppm is due to Li^+ ions from residual electrolyte.

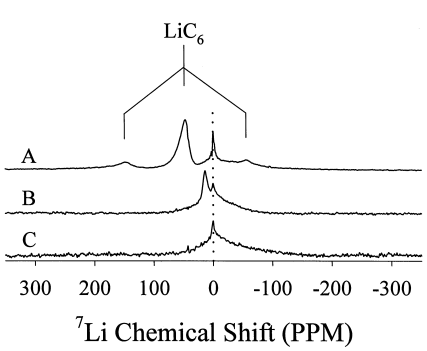

Fig. 4. Comparison of ^{7}Li NMR spectra recorded at room temperature for graphite (lithiated, A) and sepiolite-derived carbon tubes (lithiated, B; delithiated, C). One molar aqueous fill was used as an external chemical shift reference for 0 ppm.

A fourth spectral signature for intercalated lithium was only seen once before. It was reported for corannulene, which is a discrete molecular compound with a curved ring system. Corannulene is not accommodated by any of the above spectral signatures because the 47, 100, and 20 ppm features were all absent from the lithiated corannulene electrode material despite the fact that the corannulene electrode contained a high intercalated lithium content as metered by the high reversible capacity that was found for the corannulene electrodes [21]. Instead, the lithium-intercalated corannulene exhibited a complex spectrum with several broad features that extended over a 2000 ppm range. This was interpreted as due to a contact shift that results from the unpaired electrons that are predicted by the molecular orbital calculations for lithiated corannulene. For comparison, resonance shifts that are similar in magnitude have been reported for ^{6}Li in lithium manganate cathode materials [47]. The carbon tubes that were synthesized from sepiolite also exhibit broad spectral features that extend over a 2000 ppm range when investigated with a large spectral window. Notably, the baseline of the lithiated graphitic carbon is extremely flat using identical spectrometer settings and the same NMR cell. The molecular orbital calculations predict orbital multiplicities of 2 or 4 for carbons with curved lattices. The measured pore size for the sepiolite-derived carbon is 6.8 ± 0.5 Å, which is consistent with a curved lattice structure. Hence, to date, there are two such carbon materials that have been investigated by ^{7}Li NMR spectroscopy, corannulene and the sepiolite-derived carbon tubes. Both carbons exhibit complex ^{7}Li spectral features that are substantially different from that of any other carbon. In addition, the sepiolite-derived carbon tubes are different from the corannulene in that the carbon tubes also exhibit the 20 ppm signature that is commonly observed for many carbons. In contrast, the corannulene is a discreet molecular model compound and contains no discernable feature in the 5–20 ppm range.

The ^{7}Li NMR spectrum of a sepiolite-derived carbon sample that was cycled 5 times and left in the delithiated stage (OCV = 1.211 V) is shown in trace C of Fig. 4. The spectrum depicts a broad asymmetric resonance centered near 0 ppm. This result is consistent with previously reported spectral signatures for irreversible lithium in soft carbons [42]. It is noteworthy that the integrated spectral intensity over a 400 ppm range for sepiolite-derived carbon was substantially smaller than that observed for graphite. Thus, the vertical scale for traces B and C are 40 and 80 times larger, respectively, than for trace A. However, as noted above there is substantial spectral intensity distributed across a larger spectral region for the sepiolite-

derived carbon samples, which may account for lithium with a signature similar to that observed for corannulene.

There was no indication of metallic lithium dendrites in any of the carbon samples as evidenced by the lack of a signal near 260 ppm. It is noted that if the NMR coin cell were operated in a true in situ electrochemical cell configuration, then there would be a strong metallic lithium signal in the ^{7}Li NMR spectra due to the presence of the lithium foil counter electrode. It should be possible to address this issue by isolating the working electrode from the rest of the electrochemical cell using NMR imaging methods as demonstrated below, where it is shown that it is possible to resolve lithium dendrites that form on a carbon working electrode despite the presence of a large metallic lithium counter electrode. The experiment was conducted with the cylindrically symmetric cell in Fig. 2, where the radio frequency B_1 field is well defined. Additional calibration work is required before this type of imaging experiment can be conducted with the new coin cell geometry.

3.3. Lithium dendrite imaging

The application of the rotating frame NMR imaging method for in situ electrochemical system was recently developed utilizing the special geometric features of toroid cavity resonators [24,26]. The method provides high-resolution NMR spectral information as a function of the distance from the working electrode. The achievable distance resolution is on the micron scale near the working electrode. The toroid cavity resonator produces a well-defined gradient in the radio frequency magnetic field, B_1, that is produced by the NMR transmitter pulse. Accordingly, the amount of energy that is absorbed/transmitted by the sample varies with its location within the NMR detector because the efficiency of the energy transfer process is proportional to B_1. A major advantage of the toroid cavity imaging approach to magnetic resonance imaging (MRI) is that the chemical shift information is not destroyed because the measurement is conducted within a homogeneous static magnet field, B_0. In contrast, the traditional approach to MRI proceeds by converting the chemical shift information to a measure of distance with a gradient in B_0.

The results in Fig. 5 demonstrate that it is possible to follow the growth of lithium dendrites on the surface of the carbon electrode by ^{7}Li NMR spectroscopy despite the fact that the cell contains a large quantity of lithium metal which is present at the counter electrode. In addition, the dendritic lithium exhibits a different Knight shift than the bulk lithium of the counter electrode. Further studies are planed to better understand the nature of these shifts and to see if the Knight shift is sensitive to the nucleation and growth of the lithium dendrites. This type of imaging approach for the new coin cell geometry is also under development. With appropriate calibration, it should be possible to look at the working electrode using the coin cell battery images even in the presence of large quantities of Li^{+} ions in the electrolyte and a sizable lithium foil counter electrode.

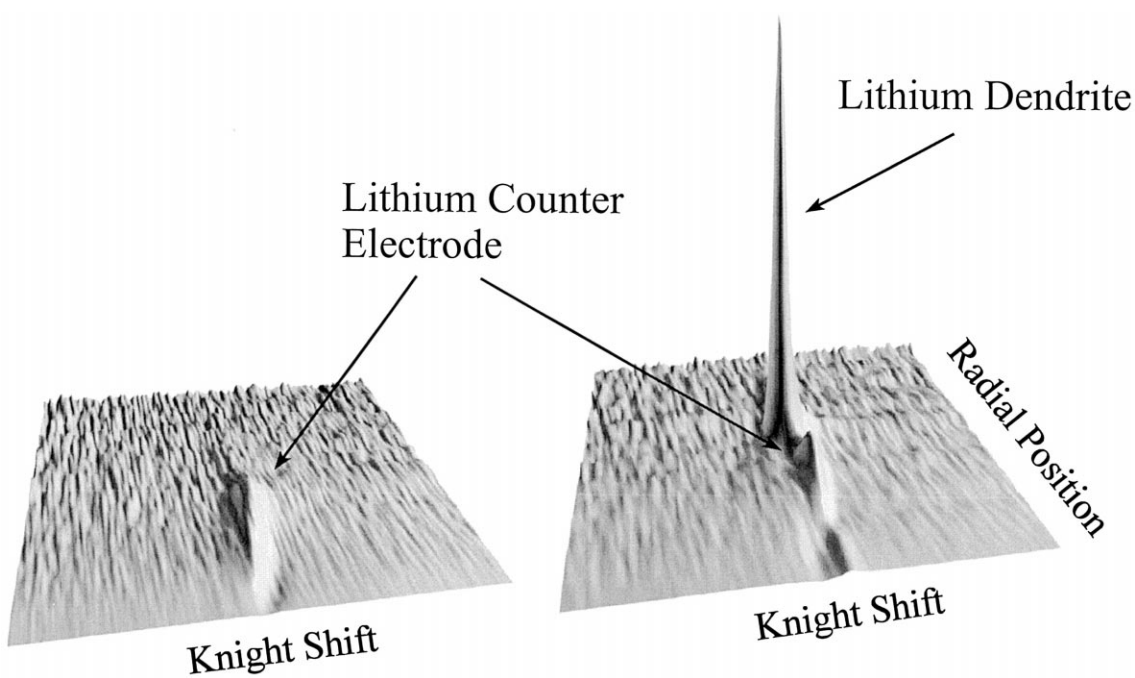

Fig. 5. ^{7}Li NMR images of the counter electrode and the lithium dendrites that were formed on a hard carbon electrode in the presence of a lithium counter electrode before (left) and after (right) passing current through the cell.

4. Conclusions

A new type of NMR detector that is well suited for analyzing the electrode components of a standard 2032-size coin cell has been developed. This NMR device exhibits remarkable ^{7}Li sensitivity even for lithiated carbon samples as small as 10 mg. This device was used to examine the synthetic carbon fibers that are produced by the pyrolytic formation of carbon in the channels of sepiolite clay. This carbon material is of interest because of its small pore size, 6.8 Å, and high reversible lithium intercalation capacity, 633 mA h/g. The sepiolite-derived carbon has no detectable graphitic character as measured by the absence of a signal at 47 ppm in the ^{7}Li NMR spectra. The NMR spectral characteristics and the reversible lithium capacity of the sepiolite-derived carbon are similar to that for lithiated corannulene. The latter species is a well-characterized discrete organic molecule with a curved aromatic ring system. Molecular orbital calculations and the NMR results are consistent with the formation of small lithium clusters within the bowl-shaped cavities afforded by the curved aromatic ring systems.

Acknowledgements

Support for this work was provided by the U.S. Department of Energy, Division of Chemical Sciences, Office of Basic Energy Sciences, under contract No. W-31-109-ENG-38.

References

[1] D. Linden (Ed.), Handbook of Batteries, 2nd edn., McGraw Hill, New York, 1995, p. 36.
[2] T. Nagaura, K. Tozawa, Prog. Batteries Sol. Cells 9 (1990) 209.
[3] G. Okuno, K. Kobayakawa, Y. Sato, T. Kawai, A. Yokoyama, Denki Kagaku 65 (1994) 226.
[4] A.M. Wilson, J.R. Dahn, J. Electrochem. Soc. 142 (1995) 326.
[5] R. Takagi, T. Okubo, K. Sekine, T. Takamura, Denki Kagaku 65 (1997) 333.
[6] N. Imanishi, H. Kashiwagi, T. Ichikawa, Y. Takeda, O. Yamamoto, M. Inagaki, J. Electrochem. Soc. 140 (1993) 315.
[7] H.H. Schönfelder, K. Kitoh, H. Nemoto, J. Power Sources 68 (1997) 258.
[8] M. Ishikawa, N. Sonobe, H. Chuman, T. Iwasaki, in: Proceedings of 35th Battery Symposium, Japan,1994, p. 49.
[9] A. Mabuchi, K. Tokumitsu, H. Fujimoto, T. Kasuh, J. Electrochem. Soc. 142 (1995) 1041.
[10] Y. Liu, J.S. Xue, T. Zheng, J.R. Dahn, Carbon 33 (1996) 193.
[11] T. Zheng, Y. Liu, E.W. Fuller, S. Tseng, U. Von Sacken, J.R. Dahn, J. Electrochem. Soc. 142 (1995) 2581.
[12] J.R. Dahn, T. Zheng, Y. Liu, J.S. Xue, Science 270 (1995) 590.
[13] P. Papanek, M. Radosavljevic, J. Fischer, Chem. Mater. 8 (1996) 1519.
[14] G. Sandí, R.E. Winans, K.A. Carrado, J. Electrochem. Soc. 143 (1996) L95.
[15] G. Sandí, K.A. Carrado, R.E. Winans, J.R. Brenner, G.W. Zajac, Mater. Res. Soc. Symp. Proc., Macroporous and Microporous Materials 431 (1996) 39.
[16] G. Sandí, R.E. Winans, K.A. Carrado, C.S. Johnson, P. Thiyagarajan, J. New Mater. Electrochem. Syst. 1 (1998) 83.
[17] G. Sandí, R.E. Gerald II, L.G. Scanlon, K.A. Carrado, R.E. Winans, Mater. Res. Soc. Symp. Proc. 496 (1998) 95.
[18] L.G. Scanlon, G. Sandí, in: Proceedings of the 38th Power Sources Conference, 1998, p. 382.
[19] L.G. Scanlon, G. Sandí, J. Power Sources (1999) (in press).
[20] J.C. Hanson, C.E. Nordman, Acta Crystallogr., Sect. B B32 (1976) 1147.
[21] G. Sandí, R.E. Gerald II, L. Scanlon, C. Johnson, R.J. Klingler, J.W. Rathke, J. New Mater. Electrochem. Syst. 3 (2000) 13.
[22] H. Azuma, H. Imoto, S. Yamada, K. Sekai, J. Power Sources 82 (1999) 1.
[23] G. Sandí, K.A. Carrado, R.E. Winans, C.S. Johnson, R. Csencsits, J. Electrochem. Soc. 146 (1999) 106.
[24] K. Woelk, J.W. Rathke, R.J. Klingler, Nuclear Resonance Tomography with a Toroid Cavity Detector, U.S. Patent 5,574,370 issued November 12, 1996.
[25] K. Woelk, R.E. Gerald, R.J. Klingler, J.W. Rathke, J. Magn. Reson., Ser. A 121 (1996) 74–77.
[26] J.W. Rathke, R.J. Klingler, R.E. Gerald, K.W. Kramarz, K. Woelk, Prog. Nucl. Magn.Reson. Spectrosc. 30 (1997) 209–253.
[27] K. Woelk, B.L.J. Zwank, J. Bargon, R.J. Klingler, R.E. Gerald, J.W. Rathke, in: P. Blümler (Ed.), Spatially Resolved Magnetic Resonance, Wiley-VCH, Weinheim, 1998, p. 103.
[28] R.E. Gerald, R.J. Klingler, J.W. Rathke, G. Sandí, K. Woelk et al., in: P. Blümler (Ed.), Spatially Resolved Magnetic Resonance, Wiley-VCH, Weinheim, 1998, p. 111.
[29] G. Sandí, R.E. Gerald II, L.G. Scanlon, K.A. Carrado, R. Winans et al., in: Materials for Electrochemical Energy Storage and Conversion: II. Batteries, Capacitors and Fuel Cells, Ginley (Ed.), MRS Symp. Proc. 496, 1998, p. 95.
[30] G. Sandí, R.E. Gerald, R.J. Klingler, J.W. Rathke, K.A. Carrado, R.E. Winans, in: Lithium Batteries, S. Surampudi, R. Marsh (Eds.), Electrochem. Soc., Proc. 98 (16)1999, pp. 400–407, New Jersey.
[31] G. Sandí, K. Song, K.A. Carrado, R.E. Winans, Carbon 36 (1998) 1755.
[32] G. Sandí, P. Thiyagarajan, K.A. Carrado, R.E. Winans, Chem. Mater. 11 (1999) 235.
[33] J. Conard, H. Estrade, Mater. Sci. Eng. 31 (1977) 173.
[34] C. Marinos, S. Plesko, J. Jonas, J. Conard, D. Guerard, Solid State Commun. 47 (1983) 645.
[35] G. Roth, K. Lüders, P. Pfluger, H.J. Güntherodt, Solid State Commun. 39 (1981) 423.
[36] Y. Dai, Y. Wang, V. Eshkenazi, E. Peled, S.G. Greenbaum, J. Electrochem. Soc. 145 (1998) 1179.
[37] N. Imanishi, K. Kumai, H. Kokugan, Y. Takeda, O. Yamamoto, Solid State Ionics 107 (1998) 135.
[38] C. Menachem, Y. Wang, J. Flowers, E. Peled, S.G. Greenbaum, J. Power Sources 76 (1998) 180.
[39] K. Tatsumi, T. Kawamura, S. Higuchi, T. Hosotubo, H. Nakajima, Y. Sawada, J. Power Sources 68 (1997) 263.
[40] S. Yamazaki, T. Hashimoto, T. Iriyama, Y. Mori, H. Shiroki, N. Tamura, J. Mol. Struct. 441 (1998) 165.
[41] S. Wang, H. Matsui, H. Tamamura, Y. Matsumura, T. Yamabe, Phys. Rev. B 58 (1998) 8163.
[42] Y. Mori, T. Iriyama, T. Hashimoto, S. Yamazaki, F. Kawakami, H. Shiroki, T. Yamabe, J. Power Sources 56 (1995) 205.
[43] N. Takami, A. Satoh, M. Oguchi, H. Sasaki, T. Ohsaki, J. Power Sources 68 (1997) 283.
[44] Y. Jung, M.C. Suh, S.C. Shim, J. Kwak, J. Electrochem. Soc. 145 (1998) 3123.
[45] Y. Jung, M.C. Suh, H. Lee, M. Kim, S.-I. Lee, S.C. Shim, J. Kwak, J. Electrochem. Soc. 144 (1997) 4279.
[46] N. Takami, A. Satoh, T. Ohsaki, M. Kanda, Electrochim. Acta. 42 (1997) 2537.
[47] Y.J. Lee, F. Wang, C.P. Grey, J. Am. Chem. Soc. 120 (1998) 12601.